ELSEVIER

A delamination mechanism for thermal barrier coatings subject to calcium–magnesium–alumino-silicate (CMAS) infiltration

C. Mercer [a,*], S. Faulhaber [a], A.G. Evans [a], R. Darolia [b]

[a] Materials Department, University of California – Santa Barbara, Engineering II, Room 1355, Santa Barbara, CA 93106, USA
[b] GE Transportation, Cincinnati, OH 45215, USA

Abstract

When a turbine airfoil attains temperatures that allow calcium–magnesium–alumino-silicate (CMAS) infiltration into the thermal barrier coating (TBC), a new mechanism of in-service spalling may be activated. The mechanism is associated with cold shock of the infiltrated layer during shut down. It has been identified by inspecting an airfoil removed from service. The identification has been based on observations of sub-surface delaminations within infiltrated regions of the TBC. Three important aspects of the mechanism are as follows. (a) The sub-surface delaminations always initiate at surface-connected vertical separations. (b) They are fully-infiltrated with CMAS. (c) They are strictly mode I. A thermal shock analysis has been invoked to identify a critical infiltration thickness, above which delaminations are possible. The analysis also defines a characteristic depth beneath the surface at which the delaminations are most likely. The observations made on the airfoils are consistent with these two dimensions. A second mechanism has been explored as the potential cause of large spalled regions also observed on the airfoils. But it has not been possible to verify the mechanism using the current observations.
© 2004 Acta Materialia Inc. Published by Elsevier Ltd. All rights reserved.

Keywords: Coatings; Delamination; Scanning electron microscopy; Residual stresses; Calcium–magnesium–alumino-silicate

1. Introduction

Yttria-stabilized zirconia (YSZ) is commonly used as a thermal barrier coating (TBC) for components located in the hot sections of gas-turbine engines [1–9]. The integrity of the coating is of paramount importance because, if spalling occurs, local hotspots are induced that accelerate degradation of the underlying bond coat and superalloy [6,9–22]. Several categories of degradation mechanisms exist.

(I) One relates to the stresses and displacements induced upon formation of the thermally grown oxide (TGO), consisting primarily of alumina.

The associated mechanisms have been widely documented [6,9–16].

(II) Another is governed by the presence of particulates in the gas turbine environment, which lead to removal of the TBC by erosion and foreign object damage. Some of the associated mechanisms have been discussed in the literature [17,18], but the understanding is still evolving.

(III) At the highest surface temperatures, calcium–magnesium–alumino-silicate (CMAS) that deposits onto the surface can penetrate the TBC, changing the near-surface mechanical properties and enhancing the spalling tendency [19–22].

The intent of the present study is to characterize the TBC on a turbine airfoil, after removal from an engine, to ascertain the role of category III under actual service conditions. The study emphasizes TBCs produced using
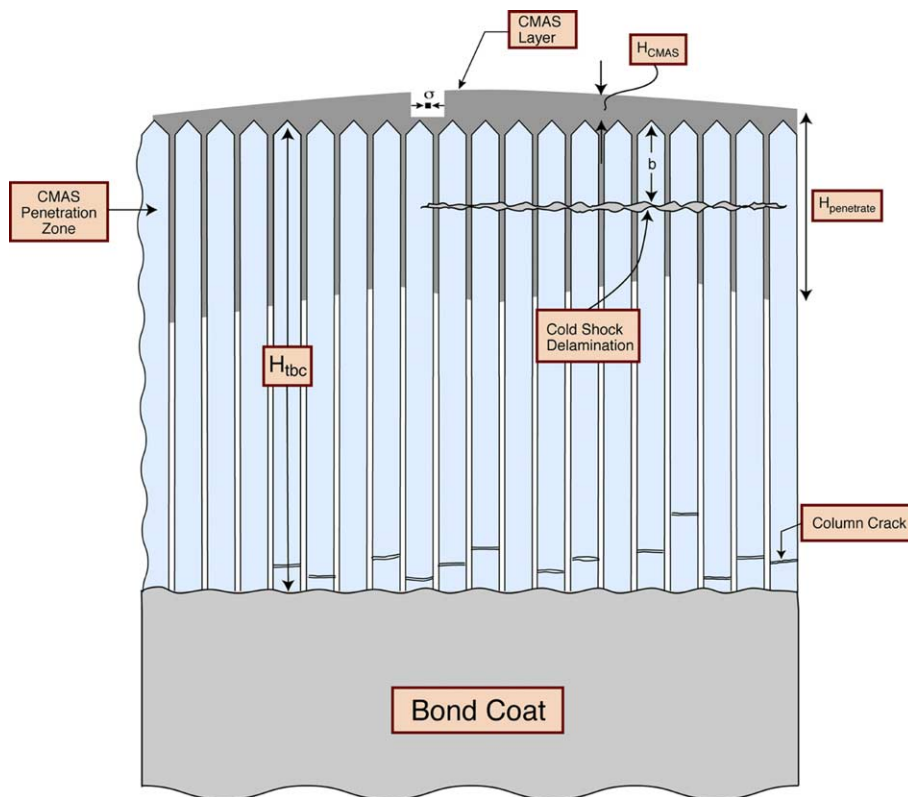
Fig. 1. A schematic of a CMAS layer that forms on the TBC and penetrates once it melts. This layer develops a large compressive stress upon cooling to ambient because of the expansion misfit with the substrate. A delamination may be induced near the base of the TBC if the energy release rate associated with the stress in the CMAS layer is high enough.

electron beam physical vapor deposition (EB-PVD), which have a strain tolerant columnar microstructure.

Category III is considered to arise because debris ingested into the engine has a chemical composition representative of CMAS [19–22]. This composition melts at $T_{\mathrm{M}}^{\mathrm{CMAS}} \approx 1240$ °C. When the TBC surface exceeds this temperature, the excellent wetting characteristics of CMAS cause it to penetrate to a depth where $T_{\mathrm{tbc}} = T_{\mathrm{M}}^{\mathrm{CMAS}}$. Thereafter, upon cooling, it solidifies as a fully-dense domain (Fig. 1). The modified thermo-mechanical properties of this region increase its susceptibility to spalling. However, the mechanism responsible for cracking and material removal is not understood. This study will identify the mechanism and provide a model characterizing the depth of the associated spalls.

2. Approach

Preliminary inspections of airfoils removed from engines are used to reveal regions where TBC spalls most commonly occur. Among the regions susceptible to TBC loss, thermal analysis is used to identify those expected to experience surface temperatures exceeding $T_{\mathrm{M}}^{\mathrm{CMAS}}$. These locations are candidates for locating spall mechanisms attributable to CMAS. In the vicinity of the spalls located in these regions, the material removal

modes on the airfoil are characterized. This is achieved by first assessing the general features on the exposed surfaces using the scanning electron microscope (SEM), as well as energy-dispersive spectroscopy (EDS). Thereafter, sub-surface details are explored by using a focused ion beam (FIB) instrument with imaging capabilities. Finally, polished cross-sections are prepared in specific regions, and also examined using the SEM. The characterizations are combined to establish the most likely material removal mechanisms. Following identification, models are used to determine the delamination energy release rates, for comparison with the toughness of the TBC. In this manner, the most likely mechanism is identified and strategies for suppressing spalling by this mechanism are discussed.

3. Characterization methods

Initial examination was performed using a JEOL 6300F field-emission scanning electron microscope (FE-SEM) to assess the general features. EDS was also employed to provide compositional information in regions of interest. Thereafter, in order to observe specific subsurface features an FEI Strata DB 235 focused ion beam instrument was used to section through selected regions. The FEI 235 is a dual-beam instrument that

combines a FIB with a FE-SEM into a single workstation. Sectioning is performed using a beam of Ga^+ ions from a liquid metal source, operated at 30 kV, with a beam diameter of 5 nm. In this study, a 5 nA beam current, normal to the blade surface, was employed to mill stair-step trenches, typically 20 μm long, 10 μm wide and 10 μm deep. In some cases, a layer of Pt (∼1 μm thick) was deposited over the region to be sectioned, in order to protect the surface from milling damage. Following milling, the sectioned face of the trench was polished using a beam current of 300 pA. Imaging was performed using the electron beam operated at 5 kV. The orientation of the electron beam (relative to the ion beam) allows simultaneous observation of the surface of the material and the sectioned face.

Cross-sections through regions of interest were prepared by grinding and polishing, utilizing a precision polishing system to maintain flatness. Micro-cloth with multi-crystalline diamond spray (3, 1 and 0.25 μm) was used for final polishing to preserve the fine structure near the TGO. After sectioning, the specimens were characterized using a combination of FE-SEM and EDS.

In selected regions of the cross-section, thin foils suitable for transmission electron microscopy (TEM) have been extracted using the FIB. These thin foils have been examined using conventional and analytic methods.

4. Observations

Initial overviews of a typical spalled region (Fig. 2) indicate an "amorphous" appearance in all locations (Fig. 2(b)). This appearance differs markedly from that found in unaffected regions of the TBC (Fig. 2(c)).
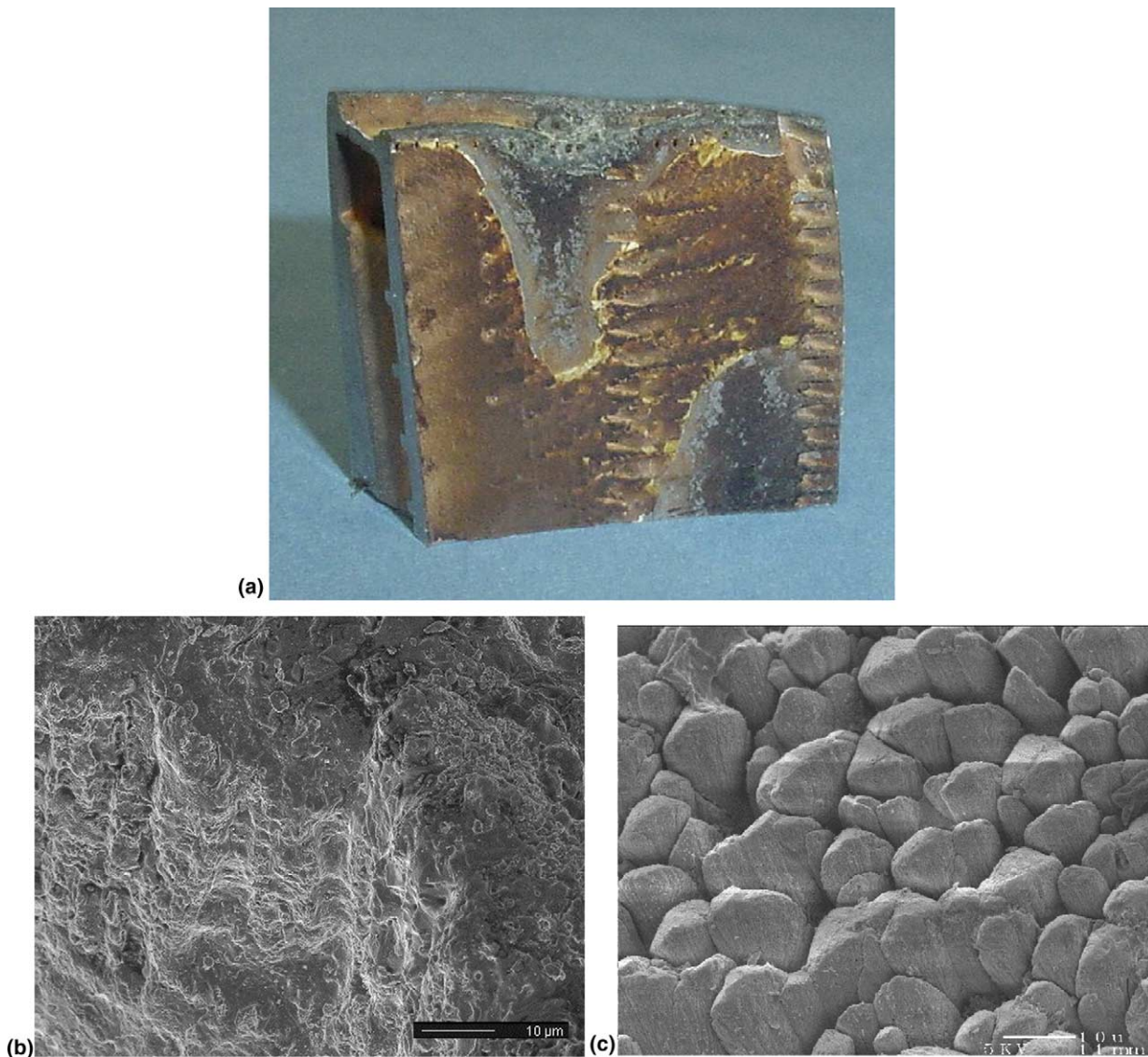

Fig. 2. (a) An optical image of the airfoil showing the spalled region to be investigated. (b) Typical spalled region exhibiting an "amorphous" appearance. (c) An unaffected region of the TBC.

Energy-dispersive spectroscopy (Fig. 3) reveals a predominance of Ca, Mg, Al, Si and O indicative of CMAS. Greater insight is provided by FIB cross-sections. In regions where the TBC has been removed, these sections (Fig. 4(a)) affirm that the CMAS is in direct contact with the TGO. In some locations (Fig. 4(b)), the remnant TGO is extremely thin, <0.5 μm thick (compared with 1–2 μm elsewhere in the airfoil), indicating that it has been dissolved by the CMAS. This observation implies that he CMAS was molten and accordingly, that this region experienced temperatures $T > T_M^{CMAS}$. Moreover, we note that the TBC columns in direct contact with the CMAS are also dissolved within a several micrometer thick layer [23]. There is no evidence that this thin layer influences delamination. Comparable sections in regions where the TBC is still in-
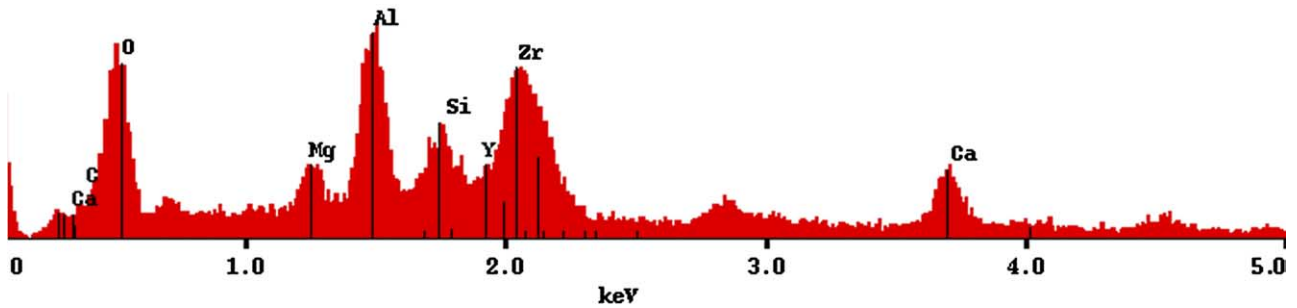

Fig. 3. EDS spectrum taken from a region where the TBC has been fully removed showing presence of CMAS elements.
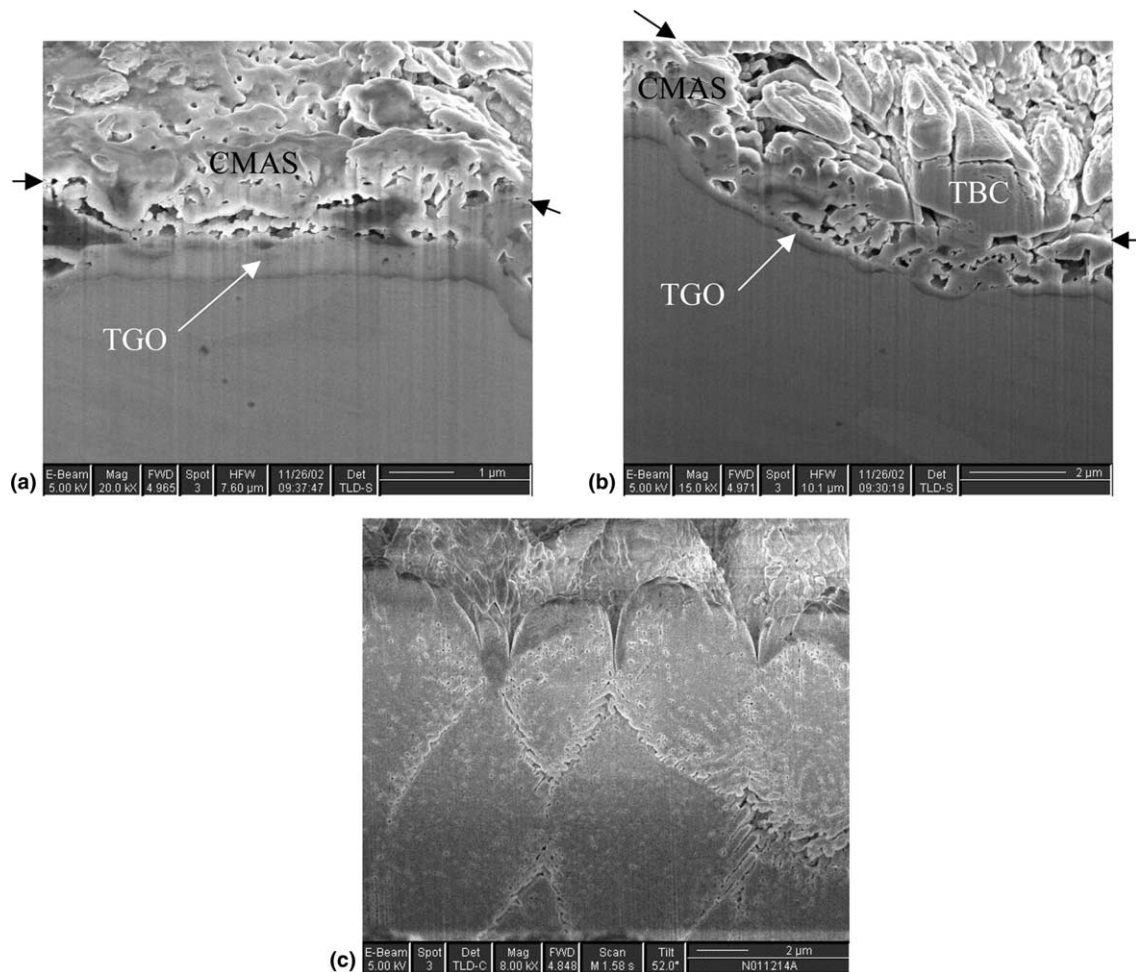

Fig. 4. (a and b) FIB cross-sections taken through CMAS in severely eroded region of blade showing (a) CMAS in direct contact with TGO and (b) CMAS beginning to dissolve TGO (arrows show edge of sectioned face). (c) FIB cross-section through undamaged TBC columns.
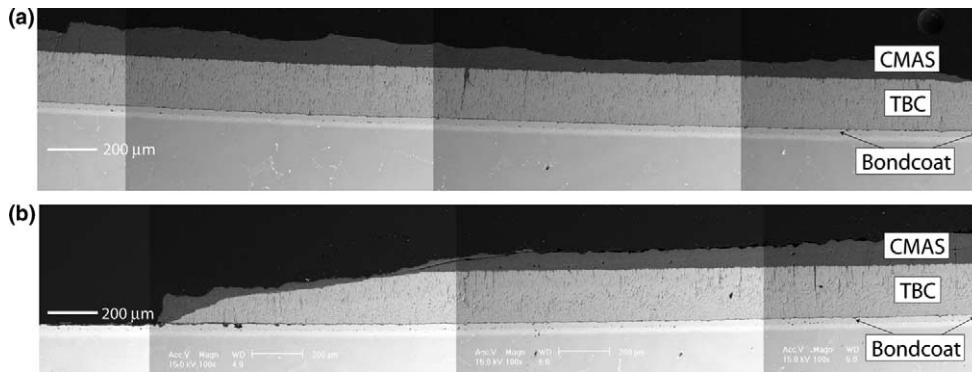
Fig. 5. Low-magnification backscattered electron image of damaged/unspalled region, (a) intact TBC, (b) region with tapered TBC.

tact (Fig. 4(c)) reveal the well-established feathery microstructure.

Polished cross-sections provide a superior perspective. A general overview at low resolution (Fig. 5) affirms that a layer of CMAS exists at all locations. Where the TBC is fully-intact, it has thickness, 20 μm < H_{CMAS} < 160 μm, and where completely removed, 5 μm < H_{CMAS} < 20 μm. Corresponding images acquired in secondary electron mode (Fig. 5) reveal a correlation between CMAS layer thickness and the depth of penetration, $H_{penetrate}$. Namely, where the CMAS is relatively thick ($H_{CMAS} \approx 120$ μm) the penetration is quite shallow ($H_{penetrate} \approx 40$ μm). Conversely, where the CMAS is thinner ($H_{CMAS} \approx 30$ μm), the penetration is much deeper ($H_{penetrate} \approx 120$ μm). Higher resolution images affirm that, in the penetrated region, CMAS is present between all of the TBC columns (Fig. 6(b)): while below that region, the inter-columnar gaps and feathery structure (typical of the as-deposited TBC) remain in evidence (Fig. 6(c)), with no CMAS.

The most informative observations have been made in select regions where the TBC is either intact or partially removed (Fig. 7). The images reveal a multiplicity of delamination cracks parallel to the surface that originate from *surface-connected vertical separations*. The delaminations are all confined within the zone penetrated by the CMAS and all *are completely filled with CMAS*. The depths range from, 20 μm < H_{delam} < 60 μm. They are typically long, 50 μm < a_{delam} < 200 μm. The TBC beneath the penetrated region appears to be intact, with no discernable delaminations nor transcolumnar cracks.

Higher resolution images of the delaminations and of the interface between the TBC and CMAS (Figs. 7 and 8) indicate domains with differing grey scale, suggestive of multiple phases. The composition range for these phases has been obtained by using X-ray mapping (Fig. 8). The regions with dark grey contrast are deficient in Zr but contain relatively larger amounts of Mg, Si, Ca and Al. Additional information about the phases present has been obtained using transmission electron microscopy [23]. The principal finding is that the CMAS above the TBC is crystalline (probably anorthite) and contains Fe as well as Ca, Mg, Al and Si.

The images of the delaminations (Fig. 7(d)) provide additional information. They indicate that the TBC on the two sides of the crack experiences only opening (mode I) displacements. That is, the (CMAS filled) inter-columnar gaps on the two sides of the delamination remain aligned, with no shear (mode II) displacement. This observation is crucial to the following assessment of the delamination mechanism.

5. Delamination mechanisms

The presence of mode I delaminations parallel to the surface, entirely within the CMAS penetrated layer (originating at surface-connected vertical separations), suggests the cold shock mechanism depicted on Fig. 9 [24]. The basic context is as follows.

(i) Upon cooling below 1240 °C, when the CMAS solidifies, the penetrated layer develops *composite* thermo-mechanical properties comparable to that for dense YSZ (because the inter-columnar CMAS represents a small fraction of the volume): that is, modulus, $E_{comp} \approx 200$ MPa, thermal expansion coefficient, $\alpha_{comp} \approx 11$ ppm/°C, and mode I toughness, $\Gamma_c = 45$ J m^{-2} [25].

(ii) Upon rapid cooling, during abrupt shut down, once the CMAS solidifies the high in-plane stiffness causes large, near-surface, tensile stresses, σ_{xx} [24].

(iii) The ensuing stress state is comparable to that associated with a thin film in residual tension on a thick substrate [26,27], with a corresponding propensity for delamination. Note that this only happens provided that a surface connected separation (or free edge) is present [24].

(iv) The tensile stresses induce a delamination that extends parallel to the surface at a characteristic depth, subject to a steady-state energy release rate [24,26].
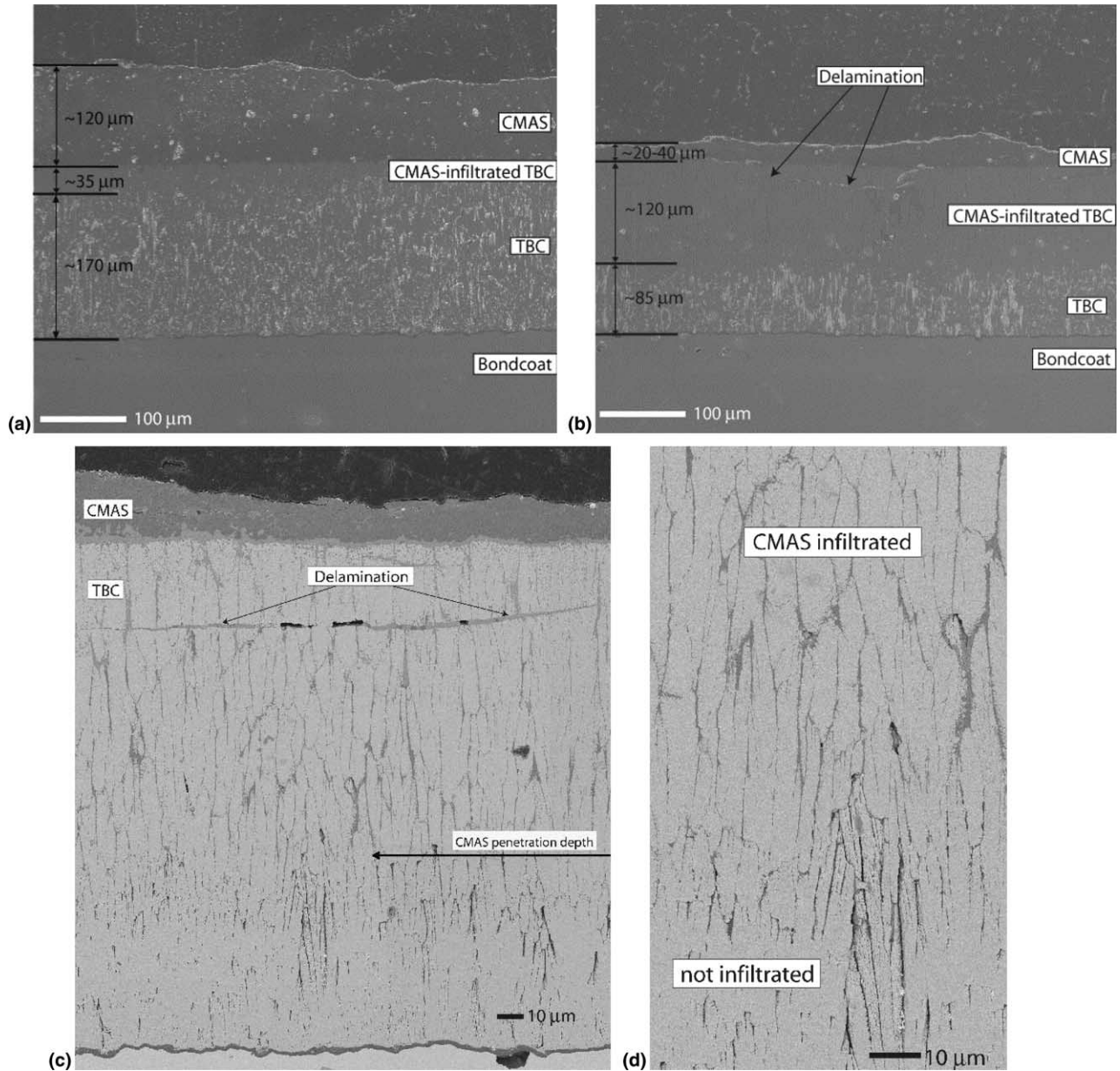
Fig. 6. (a) and (b) Low-magnification secondary electron images: (a) region with "thick" CMAS layer and shallow infiltration depth deposit, (b) region with "thin" CMAS layer and deeper penetration. (c) and (d) Backscattered electron images: (c) overview of CMAS infiltrated zone and of a delamination within this layer, (d) detail near the base of the CMAS infiltrated layer and of the unaffected TBC (the lighter grey contrast in the inter-columar gaps identifies the CMAS).

(v) Upon reheating above T_{CMAS}^M, the fluid would be drawn in by capillarity, filling the delamination.

A cold shock model describing this mechanism [24] will be invoked and evaluated below. This mechanism can generate delaminations. Spalls could be the consequence of cumulative delamination and material loss caused by sequential cold shocks.

Upon reaching ambient, an additional mechanism may arise. Now, the superposed CMAS layer develops a large in-plane compression, σ_{CMAS}, because of its high modulus, E_{CMAS}, as well as its low thermal expansion coefficient (relative to the substrate, $\Delta\alpha_{CMAS} = \alpha_{substrate} - \alpha_{CMAS} \approx 8$ ppm/°C). In the presence of an "internal" edge (such as a vertical separation caused by sintering), the stress in this layer can be partially relaxed by elongating parallel to the substrate [18]. The associated displacement causes the underlying TBC columns to experience bending and the ensuing stresses could cause column cracking. Moreover, a putative delamination emanating from the "edge" would acquire an energy release rate. If large enough, the entire TBC could be detached (over a defined region). While subcritical delaminations of this type have not been de-
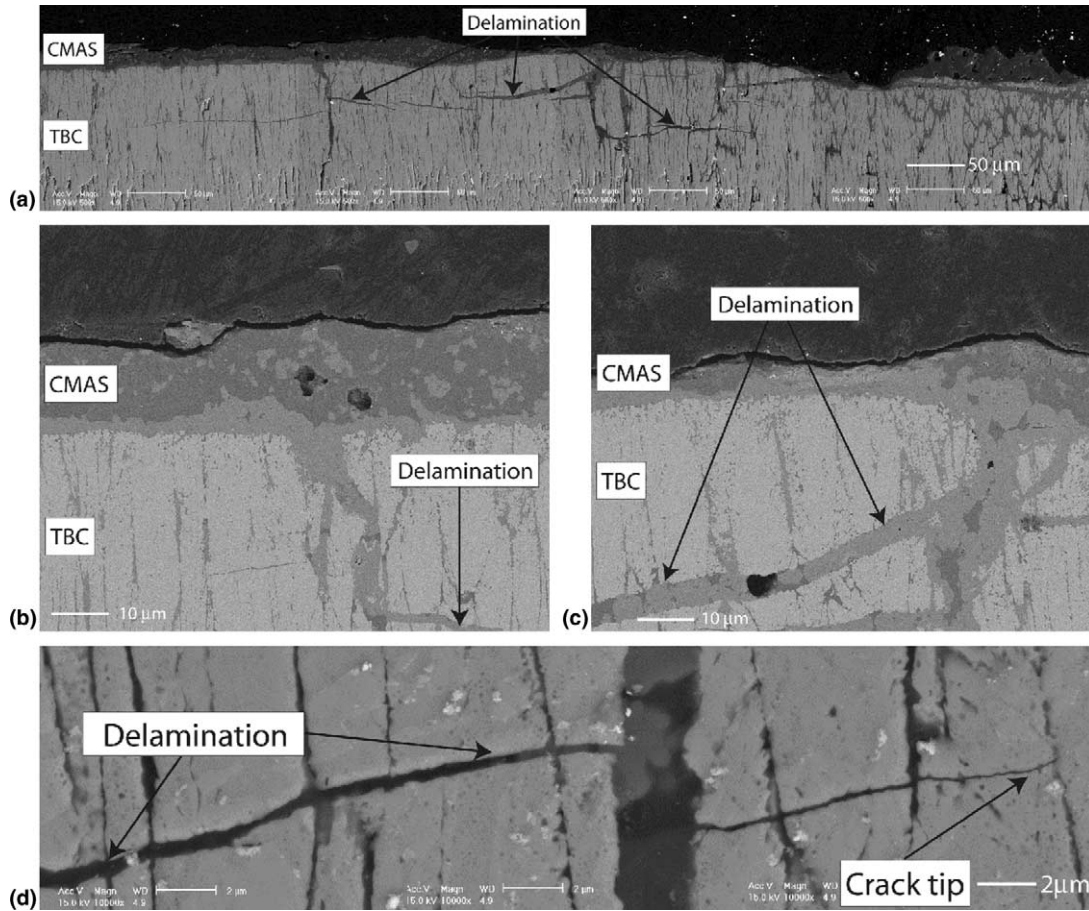
Fig. 7. (a) Low-magnification backscattered electron image of region with delamination cracks. (b) Backscattered electron image showing phase contrast at interface TBC/CMAS. (c) Backscattered electron image showing phase contrast in CMAS infiltrated crack. (d) Backscattered electron image showing CMAS infiltrated crack. Note that the inter-columnar gaps on both sides of the crack remain aligned, indicating that the delamination is strictly mode I.

tected, such a mechanism could account for large area spalls (which completely remove the TBC).

5.1. Cold shock

In cold shock situations, the material at original temperature, T_i, is instantaneously exposed to an environment at temperature, T_∞, causing a temperature gradient normal to the surface, along z. In turn, this causes in-plane tension near the surface and compression below. In such cases (for a homogeneous plate, thickness H, thermal expansion coefficient, α, modulus, E) cracking may occur either normal or parallel to the surface (or both), governed by the following suite of non-dimensional parameters [24]:

(a) Biot number, $Bi = hH/k$,
(b) reference energy release rate, $G_0 = \overline{E}\bar{\alpha}^2 H(T_i - T_\infty)^2$,
(c) time after the onset of cooling, $\bar{t} = \kappa t/H$,
(d) temperature, $\overline{T} = \frac{T(z,t)-T_\infty}{T_i=T_\infty}$,
(e) delamination depth, $\bar{b} = b/H$,

where $\bar{\alpha} = \alpha(1 + v)$, $\overline{E} = E/(1 - v^2)$, with h the heat transfer coefficient at the TBC surface: k is the thermal conductivity of the penetrated layer and κ its thermal diffusivity.

The shock requirements for forming surface connected vertical cracks are less stringent than those for forming delaminations [24]. The expectation, therefore, is that vertical cracks develop first. The critical step is the extension of the delamination. This expectation is consistent with the present observation that *all delaminations emanate from vertical separations* (albeit filled with CMAS at the time of observation). The parameters affecting delamination are: the steady-state energy release rate, G_{ss}, and the phase angle, $\Psi = \tan^{-1}(K_{II}/K_I)$, as well as the thermal boundary conditions at the base of the TBC. To obtain estimates of the critical penetration depth that causes cold shock delamination, an analysis for a homogeneous plate subject to instantaneous temperature change is used [24]. A numerical analysis that accounts for the differing characteristics of the penetrated and unpenetrated TBC layers, as well as the substrate, will be presented elsewhere [25].
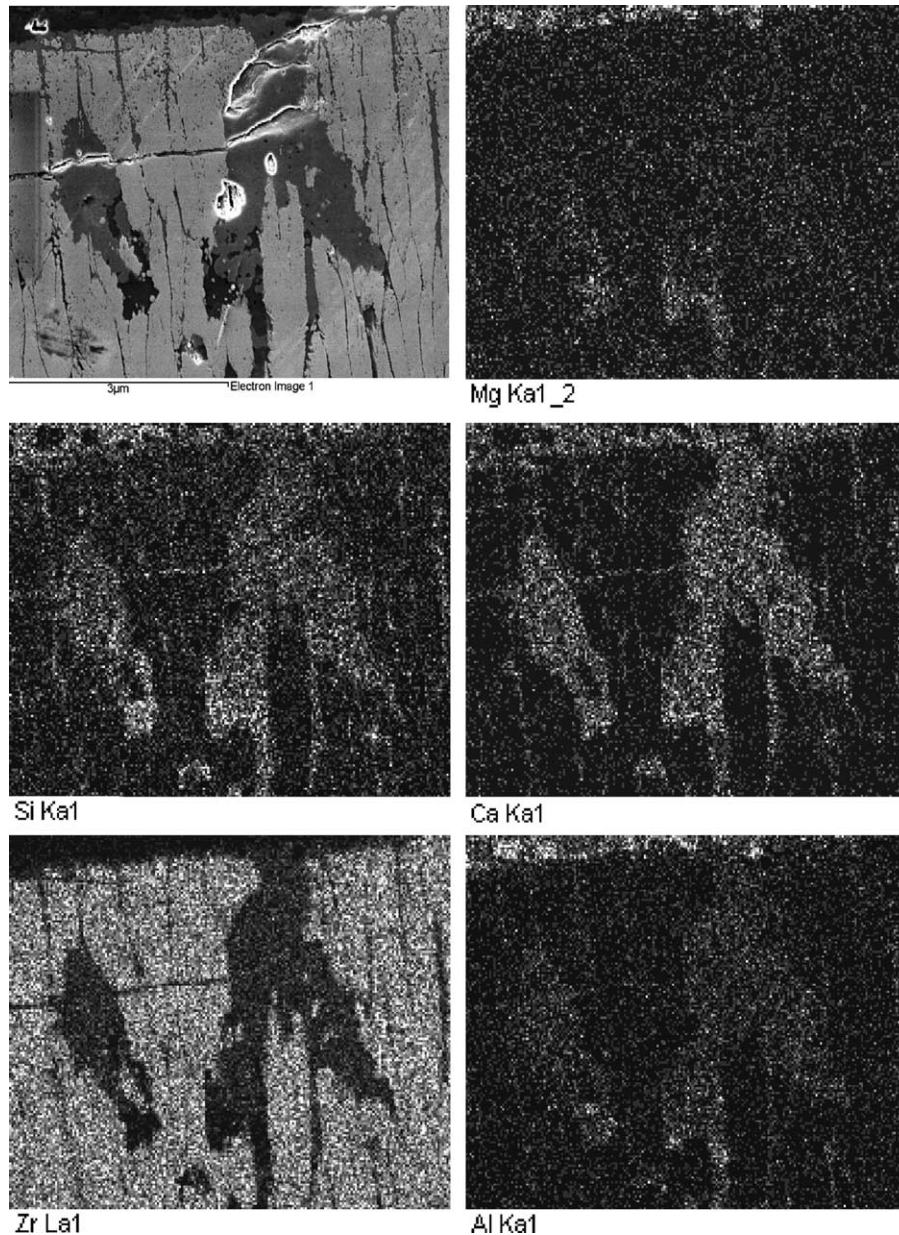
Fig. 8. X-ray map showing distribution of elements within the CMAS infiltrated regions between the TBC columns.

For a turbine airfoil under shut down conditions, it is assumed that rapid cooling occurs simultaneously at the external surface and the internal cooling holes. Deviations from this boundary condition will be explored elsewhere [15]. For simultaneous cooling, the trends in G_{ss} and Ψ for the homogeneous plate are depicted on Fig. 9. The most important feature is the existence of a subsurface delamination plane that experiences pure mode I, *regardless of the time after imposing the shock* (Fig. 9(b)). The existence of such a plane is consistent with the present observation that the delaminations are strictly mode I (Fig. 7(d)) and that cracks in brittle solids extend along planes with zero mode II [25]. This result also provides a natural delamination depth, $\bar{b} = 1/2$ (Fig. 9(b)).

For this case, the steady-state delamination energy release rate along the mode I plane is given by the following formula [24]:

$$G_{ss} = 0.08 \frac{G_o}{[1 + 2/Bi]^2}. \tag{1}$$

By using the above definition for G_o, upon equating G_{ss} to the mode I toughness of the penetrated layer, Γ_c, a critical Biot number, Bi^*, may be ascertained by solving the cubic formula

$$\frac{1}{\sqrt{Bi^*}}\left(1 + \frac{2}{Bi^*}\right) = 0.3\Lambda \tag{2}$$

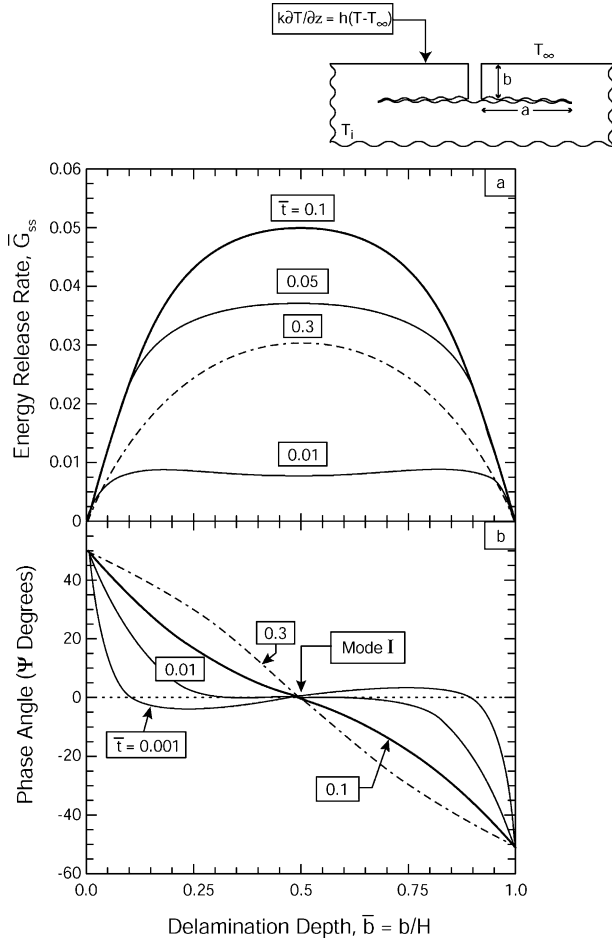with non-dimensional property parameter

Fig. 9. (a) Trends in steady-state energy release rate with delamination depth, b, plotted at several values of the non-dimensional time after initial the initial shock: for a Biot number, $Bi = 10$. Note the existence of a maximum at, $\bar{t} \approx 0.1$ and depth, $\bar{b} = 0.5$. (b) The corresponding trends in the phase angle showing that the delamination is mode I ($\Psi = 0$) at $\bar{b} = 0.5$, regardless of the time $\bar{t}$. The inset shows the configuration with a surface-connected vertical crack and a constant heat flux boundary.

$$\Lambda = \alpha_{\mathrm{comp}}(T_{\mathrm{CMAS}}^{\mathrm{M}} - T_\infty)\sqrt{\frac{E_{\mathrm{comp}}(1+\nu)}{(1-\nu)\Gamma_c}}.$$

That is, when $Bi > Bi^*$, the CMAS penetrated layer becomes susceptible to cold shock delamination. The trend in Bi^* with Λ is plotted on Fig. 10. This plot allows estimation of the critical penetration thickness, $H_{\mathrm{penetrate}}^*$, for cold shock cracking for any heat transfer condition (at least for the homogeneous plate). Upon using the following values for the properties of the TBC layer penetrated with CMAS

$E_{\mathrm{comp}} = 200$ GPa, $\quad \alpha_{\mathrm{comp}} = 11$ ppm/°C,

$\Gamma_c = 45$ J m^{-2}, $\quad \nu = 0.2$, $T_{\mathrm{CMAS}}^{\mathrm{M}} = 1240$ °C,

it is apparent that $\Lambda \approx 800$. Superposing this value onto Fig. 10 indicates that $Bi^* \ll 1$: whereupon (2) reduces to
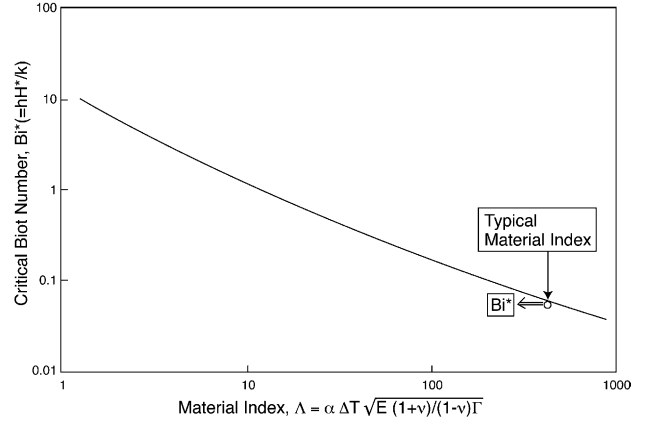
Fig. 10. Trends in the critical value of the Biot number as a function of the non-dimensional property parameter of the infiltrated layer.

$$Bi^* \approx \frac{3.6}{\Lambda^{2/3}} \tag{3a}$$

or

$$H_{\mathrm{penetrate}}^* = \frac{3.6k}{h\Lambda^{2/3}}. \tag{3b}$$

Note that the critical thickness is sensitive to the heat transfer coefficient. The implication is that there is a critical heat transfer coefficient below which cold shock cracking can be prevented. This condition is obtained by equating $H_{\mathrm{penetrate}}$ to $H_{\mathrm{penetrate}}^*$. Typical values of the heat transfer coefficient for a rapid shut down, $h = 10^3$ W/m^2 K [28] and the thermal conductivity ($k = 1$ W/m K) indicate a critical penetration, $H_{\mathrm{penetrate}}^* = 30$ μm. That is, when $H_{\mathrm{penetrate}} > H_{\mathrm{penetrate}}^*$, the layer becomes susceptible to cold shock delamination (occurring at depth, $b = H_{\mathrm{penetrate}}/2$). Recall that such delaminations only occur if a surface connected vertical crack exists at the site of the shock. All of the present observations are consistent with this lower bound. Namely, where $H_{\mathrm{penetrate}} \approx 50$ μm, delaminations indeed occur (at depth, $b \approx 30$ μm). Cold shock thus appears to be a viable mechanism of material removal once CMAS penetration has occurred. An ensuing numerical study conducted for the actual turbine airfoil will provide more specific values of $H_{\mathrm{penetrate}}^*$ [25].

5.2. Column bending and delamination

A model of column bending and delamination in the presence of "internal edges" (see Fig. 1) [18], has provided the following perspective.

(a) The TBC columns below the CMAS layer experience bending, both where they connect to the TGO and just beneath the CMAS. The bending stress, if large enough, could cause cracking on a

column-by-column basis. The damaged columns could be the source of material removal in the presence of other loads, such as particle impact.

(b) A delamination could form at the edge and extend into the TBC, causing a large-scale spall. Note that neither of these phenomena has been observed in the regions of the airfoil where the TBC is either fully or partially intact. For this case, delamination occurs preferentially *at the bottom of the TBC*: $H_{delam} = H_{tbc}$. Placing the delamination on this plane, and fixing H_{tbc}, the effect of H_{CMAS} on the steady-state energy release rate can be closely approximated by [18]

$$G_{ss} \approx 0.5\left(T_{CMAS}^M - T_\infty\right)^2$$
$$\times \left\{(\alpha_{sub} - \alpha_{tbc})^2\left[H_{tbc}E_{tbc} + H_{penetrate}(E_{comp} - E_{tbc})\right]\right.$$
$$\left. + H_{CMAS}(\alpha_{sub} - \alpha_{CMAS})^2 E_{CMAS}\right\}. \tag{4}$$

Assuming that $E_{CMAS} \approx 100$ GPa (representative of oxide glasses) and that $\alpha_{sub} - \alpha_{CMAS} \approx 8$ ppm/°C, and inserting the measured values for H_{CMAS} (100 μm) and $H_{penetrate}$ (100 μm), the steady state energy release rate, G_{ss}, is found to be in the range 100–120 J m^{-2}. This compares with a mode II toughness in the range, $\Gamma_{tbc} \approx 80$–100 J m^{-2} [29]. However, the available energy release rate, G_{actual} depends on the initial length, a_{delam} of a delamination previously formed at the base of a vertical separation: for example, $G_{actual}/G_{ss} \approx 1/2$ for $a_{delam}/H_{tbc} \approx 1$ and only, $G_{actual}/G_{ss} \approx 1/4$ when $a_{delam}/H_{tbc} \approx 1/2$. When G_{actual} reaches the mode II toughness of the TBC, Γ_{tbc}, the TBC delaminates. There is no obvious rationale for forming delaminations of this size, so it remains unclear whether this represents a viable mechanism.

6. Concluding remarks

A combination of experimental observations and analysis has been used to show that when a turbine airfoil experiences temperatures that allow CMAS infiltration, a cold shock delamination mechanism is activated. Mode I sub-surface delaminations have been observed to emanate from surface-connected vertical separations having characteristics consistent with a cold shock mechanism. A shock analysis has identified a critical infiltration thickness, $H_{penetrate}^*$, above which the penetrated layer is susceptible to delamination and spalling. For a rapid shock, the model predicts a critical thickness, $H_{penetrate}^* = 30$ μm, with delaminations expected at characteristic depth, $b = H_{penetrate}/2$. For less severe shocks, the critical thickness is appreciably larger. Repeated shock of infiltrated regions could

cause large area spalls by sequential material removal. The model suggests two approaches for preventing this mechanism.

(a) Maintain the temperature within a range that assures a CMAS penetration depth below the critical thickness.
(b) Control the cooling rate during shut down to assure a Biot number (heat transfer coefficient) below the critical level.

Neither approach has much practical utility, suggesting that a materials solution be sought.

A second delamination mechanism potentially responsible for large spalls has also been investigated. It arises because the misfit between the superposed CMAS and the substrate causes bending of the underlying TBC columns and provides an energy release rate for mode II delamination from through-thickness vertical separations. However, the present observations do not provide evidence in support of this mechanism.

References

[1] Miller RA. J Am Ceram Soc 1984;67:517.
[2] Strangman TE. Thin Solid Films 1985;127:93–105.
[3] Miller RA. In: Proceedings of the thermal barrier coatings workshop, NASA CP 3312; 1995. p. 17.
[4] DeMasi-Marcin JT, Gupta DK. Surf Coat Technol 1994;68–69:1–9.
[5] Maricocchi A, Bartz A, Wortman D. In: Proceedings of the thermal barrier coatings workshop, NASA CP 3312; 1995. p. 79.
[6] Wright PK, Evans AG. Curr Opin Solid State Mater Sci 1999;4:255–65.
[7] Wright PK. Mater Sci Eng A 1998;245:191–200.
[8] Stiger MJ, Yanar NM, Topping MG, Pettit FS, Meier GH. Z Metallk 1999;90:1069–78.
[9] Evans AG, Mumm DR, Hutchinson JW, Meier GH, Pettit FS. Prog Mater Sci 2001;46(5):505–53.
[10] Sergo V, Clarke DR. J Am Ceram Soc 1998;81:3237–42.
[11] Tolpygo VK, Clarke DR. Acta Mater 2000;48(13):3283–93.
[12] Mumm DR, Evans AG, Spitsberg IT. Acta Mater 2001;49(12):2329–40.
[13] Karlsson AM, Evans AG. Acta Mater 2001;49(10):1793–804.
[14] Karlsson AM, Levi CG, Evans AG. Acta Mater 2002;50:1263–73.
[15] He MY, Evans AG, Hutchinson JW. Acta Mater 2000;48(10):2593–601.
[16] Choi SR, Hutchinson JW, Evans AG. Mech Mater 1999;31:431–47.
[17] Bruce RW. Tribol Trans 1998;41:399–410.
[18] Chen X, Wang R, Yao N, Evans AG, Hutchinson JW, Bruce RW. Mater Sci Eng A 2003;352(1–2):221–31.
[19] Borom MP, Johnson CA, Peluso LA. Surf Coat Technol 1996;86–87:116–26.
[20] Kim J, Dunn MG, Baran AJ, Wade DP, Tremba EL. Trans J Eng Gas Turbines Power 1993;115(3):641–751.
[21] Stott FH, de Wet DJ, Taylor R. In: Froes et al., editors. Manchester: SAMPE, vol. 3; 1992. p. M92–101.
[22] Smialek JL, Archer FA, Garlick RG. In: Froes et al., editors. Cleveland, OH: SAMPE, vol. 3; 1992. p. M63–77.

[23] Krämer S, Yang J, Levi CG. Thermochemical interactions of TBCs with molten CMAS; 2004, to be published.

[24] Zhao LG, Lu TJ, Fleck NA. Mech Phys Solids 2000;48:867–97.

[25] Watanabe M, Mercer C, Levi CG, Evans AG. Acta Mater 2004;52:1479–87.

[26] Suo Z, Hutchinson JW. Int J Solids Struct 1989;25(11):1337–53.

[27] Drory MD, Thouless MD, Evans AG. Acta Metall 1988;36(8):2019–28.

[28] Darolia R. Private communication.

[29] Beuth JR. Int J Solids Struct 1992;29:1657–75.